REGULAR ARTICLE

Structural and electronic properties of tungsten trioxides: from cluster to solid surface

Hua Jin · Jia Zhu · Jianming Hu · Yi Li ·
Yongfan Zhang · Xin Huang · Kaining Ding ·
Wenkai Chen

Abstract Geometries and electronic structures of $WO_3(001)$ surface and a series of stoichiometric $(WO_3)_n$ clusters ($n = 1$–6) have been systematically investigated using first-principles density functional calculations. Six possible reconstructed models of $WO_3(001)$ surface with cubic phase are explored, and the most stable configuration is the $(\sqrt{2} \times \sqrt{2})R45°$ surface. The main feature of $WO_3(001)$ surface is that the top of valence band is dominated by the $2p$ states of the bridging oxygen atom, rather than the top terminal oxygen. By comparing the geometrical parameters, from the structural point of view, the W_3O_9 cluster can be used as the smallest molecular prototype of the WO_3 surface. However, in terms of the electronic structure, only until W_6O_{18}, the cluster begins to appear the electronic feature of the $WO_3(001)$ surface. This may be due to the reason that the W_6O_{18} cluster and the top layer of $WO_3(001)$ surface show similar "stoichiometry" if we treat two kinds of oxygen atoms as different "elements". In addition, for the chemical reactivity, using BH_3 as a probe molecule, the W_6O_{18} cluster also bears general resemblance to the $WO_3(001)$ surface, and the bridging oxygen atoms in two systems are the preferred sites for the nucleophilic reaction. Therefore, our results indicate that the W_6O_{18} cluster with a spherical buckyball structure can be viewed as the smallest molecular model to understand the properties such as catalytic activity of $WO_3(001)$ surface.

Keywords Tungsten trioxides · Clusters · Surface · Density functional theory

H. Jin · J. Zhu · Y. Li · Y. Zhang (✉) · X. Huang (✉) ·
K. Ding · W. Chen
Department of Chemistry, Fuzhou University,
Fuzhou 350108, Fujian, China
e-mail: zhangyf@fzu.edu.cn

X. Huang
e-mail: xhuang@fzu.edu.cn

J. Hu
Fuzhou Command Academy, The Chinese People's Armed
Police Force, Fuzhou 350002, Fujian, China

Y. Li
State Key Laboratory Breeding Base of Photocatalysis, Research
Institute of Photocatalysis, Fuzhou 350002, Fujian, China

Y. Zhang
Fujian Provincial Key Laboratory of Theoretical and
Computational Chemistry, Xiamen 361005, China

1 Introduction

Tungsten trioxide (WO_3) has many industrial applications and has been widely used in different fields including electrochromism, photochromism, and chemical sensors. [1–3]. Especially, tungsten oxide is an important acid–base and redox catalysts and exhibits excellent activity for many catalytic reactions; for example, it can oxides benzene and toluene into maleic anhydride and benzaldehyde, respectively. Therefore, interest in tungsten oxide has been motivated in particular by improving the catalytic activity of this important material [4–11].

Up to now, the identification of catalytic active sites at the surface of catalysts and detailed reaction mechanisms in the catalytic processes are still the challenges, which is a critical step to get insight into relationships between the structure and activity of catalysts. However, because the chemical bond formed between adsorbate and surface is

similar to a cluster-like bond, clusters are good model systems to study the physical and chemical properties of bulk catalytic surfaces [12, 13]. Therefore, as a first step to obtain comprehensive understanding the structural and electronic properties of tungsten oxide surfaces and defects, a large number of tungsten oxide clusters including the stoichiometric tungsten trioxide clusters $(WO_3)_n$ with different sizes have been investigated using photoelectron spectroscopy (PES) and density functional theory (DFT) calculations. Li et al. [14] have determined the most stable configurations of a series of $(WO_3)_n$ clusters ($n = 1$–6) using the B3LYP gradient-corrected exchange–correlation functional, and among these tungsten oxide clusters, some special efforts have been paid for $(WO_3)_3$ cluster due to the fact that it shows unusual stability [15]. Based on a combined theoretical and experimental study, Sun et al. [16] have calculated the equilibrium structures and electronic properties of $(WO_3)_n$ ($n = 1$–4), and their results indicate that $(WO_3)_4$ cluster can be seen as an embryonic form of bulk tungsten oxide, in which the W–O, W–W bond lengths, and O–W–O angles are close to those in the bulk, as well as in the HOMO–LUMO gap.

On the other hand, for WO_3 bulk, the basic building block is a simple cubic perovskite-type unit with W atom occupying the center of an octahedron, and the octahedra is corner-sharing with another one. As the temperature goes up from about 100–1,000 K, the distortion of the WO_6 octahedra is observed, and as a result of the displacement of W atom away from the center of octahedron, bulk WO_3 exhibits at least five different phases including ε-monoclinic, triclinic, γ-monoclinic, orthorhombic, and tetragonal phases as the temperature increased [17–22]. However, it is commonly accepted that at room temperature, WO_3 has a γ-monoclinic lattice [23, 24]. For the γ-monoclinic phase, the single crystal (001) surface is thermodynamic stable and has been considered as a well-defined model catalyst system to explore the catalytic behavior of tungsten trioxide [17]. Many experimental investigations have been performed to characterize properties of $WO_3(001)$ surface using different technologies, such as low-energy electron diffraction (LEED), ultraviolet photoelectron spectroscopy (UPS), and scanning tunneling microscope (STM), etc. [17, 25, 26]. These previous works showed that the (001) surface appears reconstruction with the half a monolayer of the top oxygen atoms missing alternately along [100] and [010] directions, to avoid the surface dipole [27, 28]. However, theoretically, only few attentions have been paid on the structural and electronic properties of the WO_3 surface [23, 29]. Early to 1996, Oliver et al. [29] have firstly investigated the configurations of (001) surface for cubic WO_3 using the METADISE codes [30] which bases on empirical Buckingham potential to determine the

interatomic forces, and their results indicated that the $(\sqrt{2} \times \sqrt{2})R45°$ reconstructed structure is most stable. Recently, Yakovkin et al. [23] have studied the stability and relaxations of the ε-monoclinic $WO_3(001)$ surface with various types of termination, and the reasons for the surface relaxation were focused in their work. Furthermore, the DFT calculations have also been carried out to study the interactions of hydrogen and methanol molecules with the (001) surface of ε-monoclinic phase, as well as the photo-oxidation of water on γ-monoclinic WO_3 surface [31, 32]. Consequently, further theoretical studies on $WO_3(001)$ surface are necessary to get better understanding of the differences between $(WO_3)_n$ clusters and WO_3 solid surface, as well as the chemical properties of this important catalyst.

In this paper, we examine the configurations and electronic structures of tungsten trioxide clusters and solid surface using density functional calculations. We first present the surface configuration, thermodynamics stability, and electronic structure of $WO_3(001)$ surface with six possible reconstructed structures, and the result shows that the tendency of surface reconstruction of $WO_3(001)$ surface and several reconstructed structures may be coexisted. Next, the stoichiometric $(WO_3)_n$ clusters with different sizes are investigated, and by comparing the structural and electronic properties of cluster with the results of $WO_3(001)$ surface, we want to answer the question what is the critical size for the tungsten oxide cluster bearing resemblance to the surface? Finally, we choose BH_3 molecule as a typical Lewis acid to probe the basicity of different kinds of oxygen atoms on the $WO_3(001)$ surface as well as in the corresponding $(WO_3)_n$ cluster.

2 Computational details

First-principles calculations based on DFT were carried out utilizing the Vienna ab initio simulation package (VASP) [33, 34], and the ultrasoft pseudopotentials were used to describe the interaction between the ion cores and valence electrons. The generalized gradient approximation Perdew–Wang (PW91) exchange–correlation functional was employed [35], and the kinetic cutoff energy for the plane-wave expansion was set to 400 eV. In the calculations, the convergence energy threshold for self-consistent iteration was set at 10^{-4} eV, and the residual atomic forces were smaller than 0.03 eV/Å.

A periodic slab model with five layers was adopted to simulate the $WO_3(001)$ surface, and each layer consists of three atomic planes, namely the O–WO_2–O layer. During the structural optimization, as shown in Fig. 1, the top three layers were allowed to relax in all directions while atoms on the remaining two layers were constrained to the bulk

Fig. 1 Schematic side views of the WO₃(001) surface with **a** cubic phase and **b** γ-monoclinic phase. It is noted that to avoid the dipole perpendicular to the surface, half of the top oxygen atoms are moved to the bottom of the slab. The *blue* and *red spheres* indicate the W and O atoms, respectively
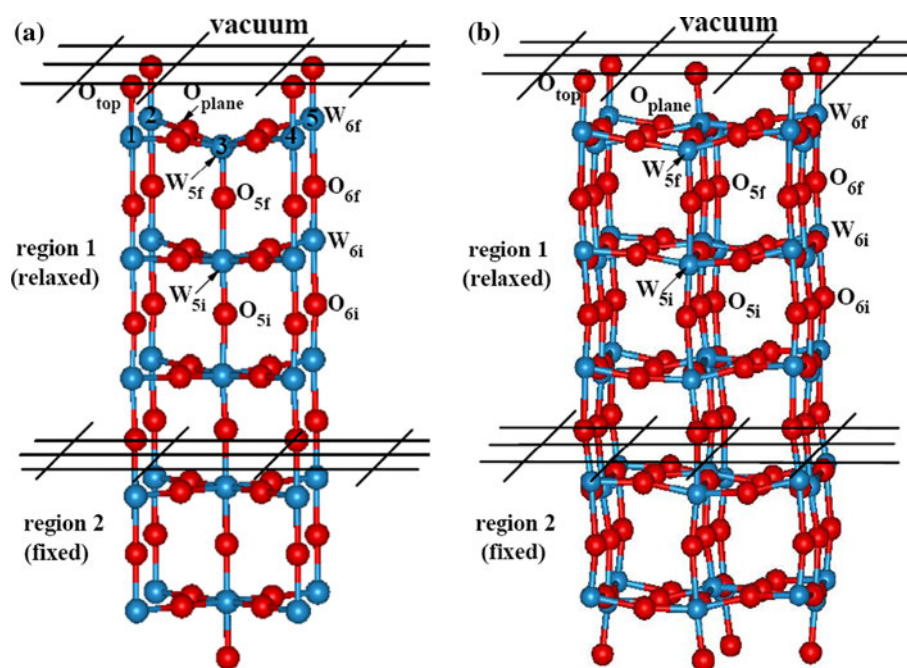
position. We have also studied the surface configurations of slabs with seven-layer and nine-layer thickness for $(\sqrt{2} \times \sqrt{2})R45°$ surface, and the results indicated the same trend on the direction of atomic displacement which was only a small influence on the positions of surface atoms. Hence, a slab with five-layer thickness (about 20 Å) was enough to obtain the properties of our interest. In addition, we have checked the effect of the vacuum width, and a vacuum width of 10 Å was sufficient for avoiding interactions between the adjacent slabs. According to the surface area of reconstructed structures, different sizes of Monkhorst–Pack k-point meshes [36] were used. Further test calculations were performed to check the effect of the spin polarization; however, there was nearly no difference between the spin-up and spin-down density of states (DOSs), and the total energy for the spin-polarized surface was almost the same as the non-spin-polarized one. So all the results reported in this work were derived from the non-spin-polarized calculations. For the stoichiometric tungsten oxide clusters, similar setting of calculations was employed, except that the cluster was placed in a $20 \times 20 \times 20$ Å cubic box and only Γ-point was considered.

In order to help the subsequent discussion, we use symbols W_{6f}, W_{5f}, O_{top}, and O_{plane} to denote the sixfold and fivefold coordinated tungsten atoms, the top terminal oxygen, and the in-plane (or bridging) oxygen atoms at the first layer (see Fig. 1), respectively. Furthermore, the oxygen atoms located just under the W_{6f}, W_{5f} atoms are labeled by O_{6f}, O_{5f}, respectively.

3 Results and discussion

3.1 Stability of reconstructed WO₃(001) surfaces

According to the atomic compositions of two outmost surfaces of slab, there are two possible terminations for the stoichiometric WO₃(001) surface. In the first case, the compositions of two outmost layers are different, namely, a monolayer composed of oxygen atoms for the top layer and a composition of WO₂-terminated surface for the bottom layer. Since in this arrangement there must be residual charges on the surface, which results in dipole perpendicular to the (001) surface, it is not energetically stable. In another case, half of the oxygen atoms on the top layer are transferred to the bottom of the slab (see Fig. 1), and the compositions of top and bottom layers are the same. Because of eliminating the dipole perpendicular to the surface, the stoichiometric WO₃(001) surface prefers this arrangement [29]. Therefore, the WO₃(001) surfaces considered in following sections are constructed by this method.

As presented in Fig. 2, six possible reconstructed WO₃(001) surfaces, including (2×1), (2×2), $(\sqrt{2} \times \sqrt{2})R45°$, $(2\sqrt{2} \times 2\sqrt{2})R45°$, (4×2), and (4×4) surfaces are investigated in the present work, and the corresponding construction units are marked in the figure. The WO₃ bulk with ideal ReO₃-like structure (cubic phase with an optimized lattice constant of $a = 3.837$ Å) is used to simulate above surface reconstructions although WO₃ has a γ-monoclinic lattice at room temperature. The reason is due

Fig. 2 Top views of the optimized configurations for six possible reconstructed $WO_3(001)$ surfaces with cubic phase, including **a** $(\sqrt{2} \times \sqrt{2})R45°$, **b** (2×1), **c** $c(2 \times 2)$, **d** (4×2), **e** (4×4), and **f** $(\sqrt{2} \times \sqrt{2})R45°$ models. In the pictures, the top oxygen, the in-plane oxygen, and tungsten atoms are denoted by *gray*, *red*, and *blue spheres*, respectively. The *solid lines* represent the corresponding construction unit of different reconstructed models. For clarity, the regions circled by *dashed line* in the picture indicate the pair of top oxygen atoms with shortest distance
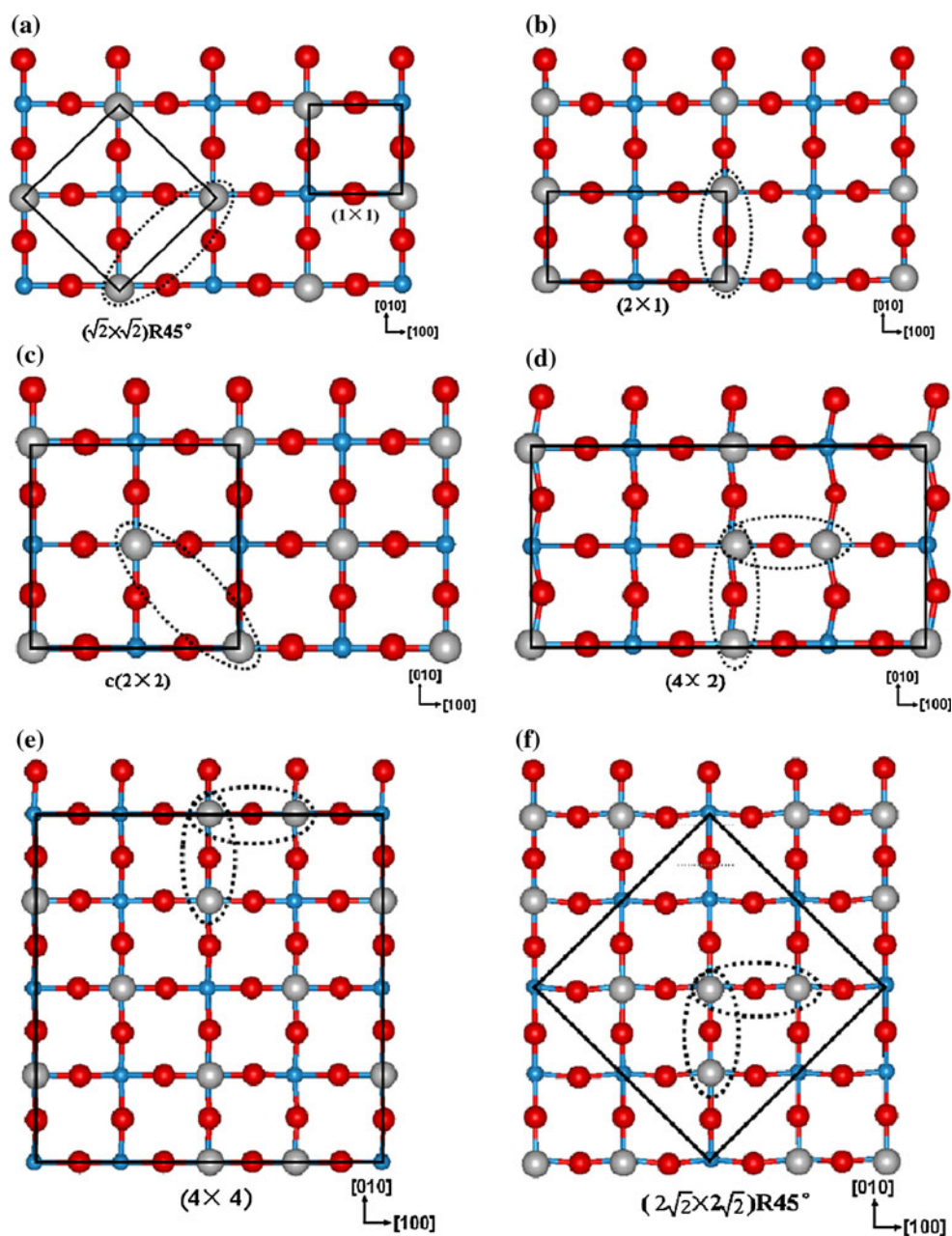
to the fact that for the large supercell, too many atoms will be involved in the calculations if the γ-monoclinic phase is used (for instance, there are 1,280 atoms for a (4×4) supercell). Actually, the cubic phase has been observed in WO_3 thin films [37, 38], and the theoretical calculations have shown that the energy difference between cubic structure and other phases is very small (<0.1 eV) [23]. To ensure the reliability of results derived from the cubic phase, the comparisons between the $WO_3(001)$ surfaces with cubic and γ-monoclinic phases will be provided after determining the most stable reconstructed model.

For further comparing the thermodynamic stability of different reconstructed structures, the surface energies (E_{surf}) are calculated, which is defined as following,

$$E_{surf} = \frac{1}{S}\left[E_{relaxed} - \frac{1}{2}\left(E_{ideal} + nE_{bulk}\right)\right]$$

where, E_{ideal}, $E_{relaxed}$, and E_{bulk} are the total energies of the ideal surface, relaxed surface, and the optimized bulk, respectively. S is the area of the surface, and n stands for the number of bulk unit found in the surface. Table 1 lists the calculated surface energies of six reconstructed

Table 1 Calculated surface energies of different restructured $WO_3(001)$ surfaces

Surface reconstruction	$(\sqrt{2} \times \sqrt{2})R45°$	(2×1)	$c(2 \times 2)$	(4×2)	(4×4)	$(\sqrt{2} \times \sqrt{2})R45°$
Surface energy (J/m^2)	0.283	1.123	0.336	1.449	0.983	0.448

$WO_3(001)$ surfaces, and the smallest surface energy (0.283 J/m^2) is obtained for the reconstructed $(\sqrt{2} \times \sqrt{2})R45°$ surface. So it seems that the reconstructed $(\sqrt{2} \times \sqrt{2})R45°$ surface is most stable, and this conclusion is in consistent with the result obtained by Oliver et al. [29], although a large surface energy (1.39 J/m^2) was predicted in this previous work. For the $c(2 \times 2)$ reconstructed surface, the corresponding surface energy (0.336 J/m^2) is only slightly larger than that of $(\sqrt{2} \times \sqrt{2})R45°$. Actually, the structural parameters of two surfaces are also very similar (not shown), and the $c(2 \times 2)$ reconstructed surface can alternatively be described as the $(\sqrt{2} \times \sqrt{2})R45°$ reconstruction (see Fig. 2) [21]. Among six models, we found that the (4×2) configuration is energetically most unfavorable. The poor stability of (4×2) surface may be due to the obvious Coulomb repulsive interactions originated from the close arrangement of top terminal oxygen atoms (see the regions circled in Fig. 2d). On the contrary, in $(\sqrt{2} \times \sqrt{2})R45°$ or $c(2 \times 2)$ surface, the reduction in Coulomb interaction can be achieved by the large separation between adjacent top oxygen atoms.

Although our results are obtained by employing the cubic WO_3, above conclusion is also suitable for the surface of monoclinic phase. It should be pointed out that in the monoclinic (001) surface, the nearly equivalent relation between the reconstructed $(\sqrt{2} \times \sqrt{2})R45°$ and $c(2 \times 2)$ surfaces (based on the ideal cubic unit cell) is not preserved because the deformation of WO_6 octahedra results in alternately long and short on-top O–O separations along the [110]

direction. Therefore, it can be expected that the $(\sqrt{2} \times \sqrt{2})R45°$ or $c(2 \times 2)$ surfaces may be the most stable reconstruction pattern for the (001) surface of monoclinic WO_3 phase. Experimentally, the $(\sqrt{2} \times \sqrt{2})R45°$ reconstruction is often appeared in the experimental results of monoclinic $WO_3(001)$ surface [17]. In addition, the $c(2 \times 2)$ reconstructed areas of the surface are also observed to coexist with $(\sqrt{2} \times \sqrt{2})R45°$ surface [21]. So, in the following sections, we will mainly focus on the properties of the $(\sqrt{2} \times \sqrt{2})R45°$ reconstruction $WO_3(001)$ surface.

3.2 Geometry of the relaxed $(\sqrt{2} \times \sqrt{2})R45°$ $WO_3(001)$ surface

Table 2 shows the atomic displacements along various crystallographic directions for the relaxed $(\sqrt{2} \times \sqrt{2})R45°$ surface with respect to the ideal cubic $WO_3(001)$ surface, and all atoms at the exposed surface tend to move outwards, except for the fivefold coordinated tungsten atom (W_{5f}). It is noted that the sixfold tungsten atom (W_{6f}) exhibits the largest relaxation (0.512 Å), and since the displacement of top terminal oxygen atom (O_{top}) just above W_{6f} is relatively small (0.304 Å), the obvious shrinking of the distance between W_{6f} and O_{top} atoms can be expected. After geometry relaxation, the length of W_{6f}–O_{top} bond decreases from 1.918 Å to about 1.710 Å (see Table 3) and now possesses a double-bond character. In addition, the outward movement of W_{6f} results in the weakness of another opposite W–O bond just under W_{6f} atom (namely W_{6f}–O_{6f} bond), which is elongated

Table 2 Surface displacements (Å) along different directions for the relaxed cubic $(\sqrt{2} \times \sqrt{2})R45°$ and γ-monoclinic $WO_3(001)$ surfaces with respect to the corresponding ideal surfaces

Surface	Cubic $(\sqrt{2} \times \sqrt{2})R45°$			γ-Monoclinic		
Direction	[001][a]	[010]	[100]	[001]	[010]	[100]
O_{top}[b]	0.304	0.000	0.047	0.106 (0.132)[c]	0.018 (0.066)	0.061 (0.051)
W_{6f}	0.512	0.000	0.000	0.160 (0.194)	0.031 (0.033)	0.052 (0.056)
O_{6f}	0.128	0.000	0.045	0.014 (0.024)	0.037 (0.039)	0.073 (0.037)
W_{6i}	0.266	0.000	0.033	0.014 (0.018)	0.007 (0.010)	0.079 (0.012)
O_{plane}	0.249	0.000	0.000	0.062 (0.058)	0.174 (0.187)	0.038 (0.029)
W_{5f}	−0.105	0.000	0.000	−0.046 (0.053)	0.040 (0.055)	0.068 (0.061)
O_{5f}	0.063	0.000	0.050	−0.033 (0.028)	0.019 (0.026)	0.018 (0.068)
W_{5i}	−0.131	0.000	0.034	−0.043 (0.051)	0.007 (0.009)	0.011 (0.086)

[a] The negative and positive values indicate that the atom moves toward the bulk and vacuum sides, respectively

[b] The symbols shown in table are illustrated in Fig. 1 and text

[c] In γ-monoclinic $WO_3(001)$ surface, two O_{top} atoms are not equivalent, as well as for other surface atoms

Table 3 Lengths (Å) of W–O bonds along the [00$\bar{1}$] direction of the cubic and γ-monoclinic WO$_3$(001) surfaces

	W$_{6f}$–O$_{top}$	W$_{6f}$–O$_{6f}$	W$_{6i}$–O$_{6f}$	W$_{5f}$–O$_{5f}$	W$_{5i}$–O$_{5f}$
Cubic ($\sqrt{2} \times \sqrt{2}$)$R45°$	1.710	2.303	1.782	1.751	2.113
γ-Monoclinic	1.711	2.332	1.774	1.749	2.179

to 2.303 Å. On the other hand, the decreasing in the length of W$_{5f}$–O$_{5f}$ bond is found because of the inward relaxation of W$_{5f}$ atom, and corresponding bond length (1.751 Å) also means the double-bond property of the W$_{5f}$–O$_{5f}$ bond. Because of the diverse atomic movements, the distances between tungsten and oxygen atoms (W–O bond) are not equal but emerge alternately short and long arrangement along the [00$\bar{1}$] direction(see Table 3). Similar distribution of the W–O bond length is also observed in the results of recent DFT study on the ε-monoclinic WO$_3$(001) surface [23]. Furthermore, the displacement of surface atom also leads to the wrinkling of the surface. For the ($\sqrt{2} \times \sqrt{2}$)$R45°$ WO$_3$(001) surface, the bond angles among surface tungsten atoms, $\angle$W1–W3–W5 and $\angle$W2–W3–W4 (see Fig. 1), decrease from 180° to 161.7°. Due to the obvious change of the surface configuration (especially the formation of W=O double bond), the stability and electronic structure of the WO$_3$(001) surface change greatly with respect to the ideal surface.

The relaxations of other reconstructed cubic WO$_3$(001) surfaces are similar to the most stable ($\sqrt{2} \times \sqrt{2}$)$R45°$ structure. All of the six reconstructed configurations also appear the same arrangement of the W–O bonds along the [00$\bar{1}$] direction, characterized by the alternatively short and long W–O distances, and the difference of the length for the same type of W–O bond among these configurations is smaller than 0.05 Å. However, as the size of reconstructed WO$_3$(001) surfaces increases, the obvious movements of surface atom along [010] and [100] directions are also observed, which can be seen clearly in the top views of those reconstructed surfaces with large size (Fig. 2). For example, in (4 × 2) surface, the largest displacement at [100] direction for O$_{top}$, W$_{6f}$, and W$_{5f}$ atoms are about 0.22, 0.16, and 0.14 Å, respectively.

Moreover, the relaxation of the WO$_3$(001) surface with γ-monoclinic phase is also investigated, and the results are listed in Table 2 for comparisons. Similar to the cubic phase, the sixfold tungsten atoms at the top layer relax outwards and present the largest displacement, while the W$_{5f}$ atoms move toward the bulk side. However, since the distortion of the WO$_6$ octahedron in the γ phase results in the formation of zigzag W–O chains along the [00$\bar{1}$] direction (see Fig. 1b), obvious movements of surface atoms along other [010] and [100] directions are also found in γ-WO$_3$(001) surface. Although the detailed surface relaxations are different, the coordination environments of tungsten atoms in two surfaces are very similar. As shown in Table 3, the lengths of corresponding W–O bonds of two surfaces are nearly identical, as well as the $\angle$W1–W3–W5 and $\angle$W2–W3–W4 bond angles (161.7° vs. 158.5° in the γ phase).
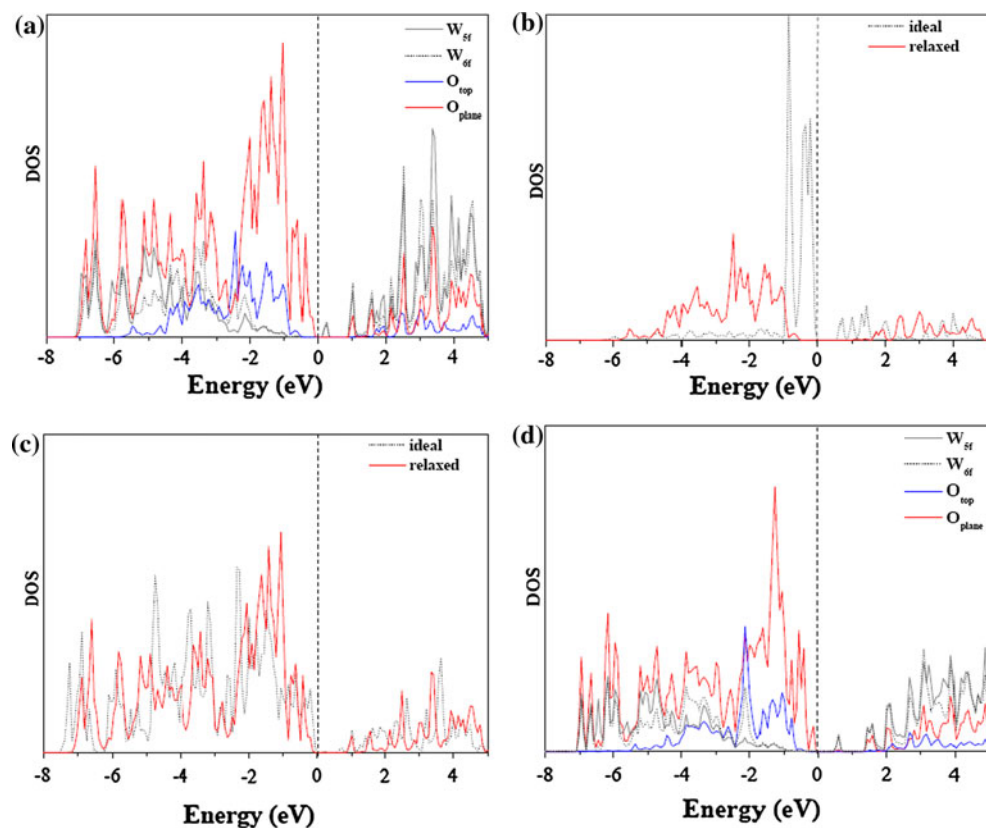
3.3 Electronic structure of the relaxed ($\sqrt{2} \times \sqrt{2}$)$R45°$ WO$_3$(001) surface

To investigate the effects introduced by the surface relaxation, in this section, we will focus on the band structure and the density of state (DOS) of WO$_3$(001) surface. For the ideal cubic surface, as shown in Fig. 3a, the semiconductor property of WO$_3$ bulk is preserved and the predicted band gap is about 0.27 eV. However, like other semiconductors, it can be expected that the band gap is underestimated due to the insufficient cancelation of the self-interaction correction inherent in the pure DFT method [39]. Further analyses show that the valence band maximum of ideal surface is dominated by the O 2p states, especially for the top terminal oxygen atoms (O$_{top}$) above sixfold tungsten atoms, and the conduction band minimum is mainly originated from the W 5d states. After surface relaxation (see Fig. 3b), because the charge redistribution near the surface gives rise to the formation of the surface state, one conduction band moves downwards and partly appears in the band gap of the ideal surface around the Γ point. According to the atomic partial DOSs displayed in Fig. 4a, the main component of surface state inside the band gap is the 5d orbitals of both W$_{5f}$ and W$_{6f}$ atoms. Another distinct feature of the relaxed WO$_3$(001) surface is that the top of the valence band is mainly composed of the 2p orbitals of the in-plane oxygen atom (O$_{plane}$). By comparing the DOSs of O$_{top}$ and O$_{plane}$ atoms in two systems (Fig. 4b, c), the surface relaxation has significant influence on the distribution the 2p states of O$_{top}$ atom, and the corresponding DOS peaks move toward the regions far from the Fermi level. Consequently, instead of O$_{top}$ atom, the top of valence band of the relaxed surface mainly contains the contributions of O$_{plane}$ atoms. The above dramatic change of the DOS near the Fermi level by the surface relaxation is also observed in the recent theoretical work of Yakovkin et al. [23], and our results reveal that the redistribution of the 2p states of O$_{top}$ atom is the reason

Fig. 3 Band structures of **a** the ideal and **b** the relaxed ($\sqrt{2} \times \sqrt{2}$)$R45°$ WO$_3$(001) surfaces. All the energies shown are reported with respect to the Fermi level
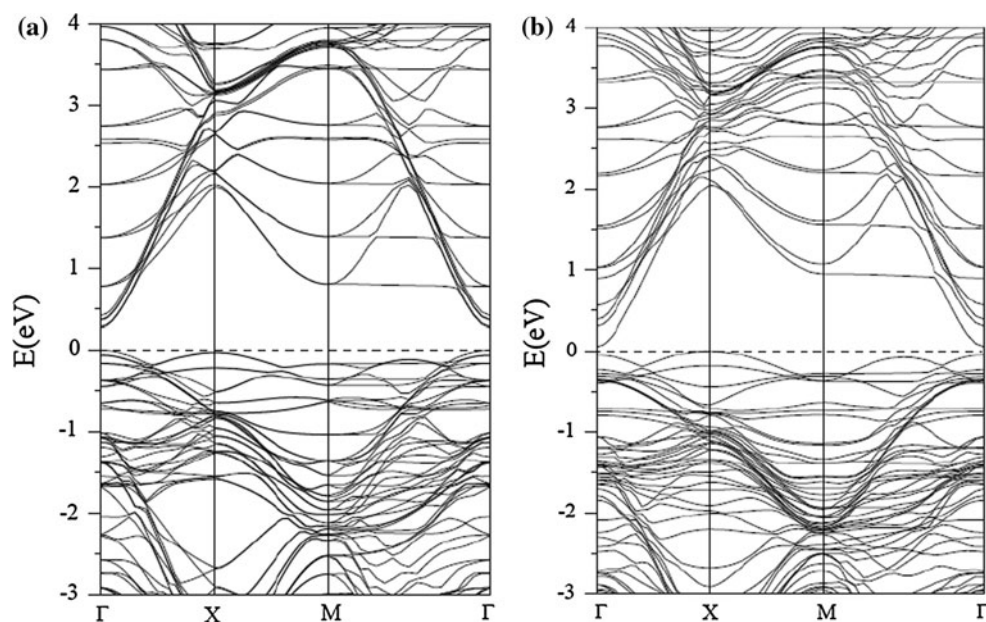
Fig. 4 Atomic DOSs of **a** the relaxed cubic WO$_3$(001) surface, **b** the top oxygen atom for the ideal and relaxed cubic surfaces, **c** the in-plane oxygen atom for the ideal and relaxed cubic surfaces, and **d** the relaxed γ-monoclinic WO$_3$(001) surface. The *vertical dashed line* indicates the Fermi level

for the disappearance of the sharp peak just below the Fermi level in the ideal surface.

As presented in Fig. 4d, the electronic structure of γ-monoclinic WO$_3$(001) surface is similar to that of reconstructed cubic ($\sqrt{2} \times \sqrt{2}$)$R45°$ surface, in which the valence band near the Fermi level is also dominated by the

$2p$ orbitals of O$_{plane}$ atoms, which is in accordance with the experimental results achieved by the valence band photoemission spectra [17, 25, 40]. It is worthwhile to note that, since the states of O$_{plane}$ tend to distribute in the region with higher energy level (or lower binding energy), the O$_{plane}$ atoms appear more Lewis basicity and nucleophilicity

than the O_{top} atoms. Therefore, the preferred sites for the nucleophilic reaction occurred at $WO_3(001)$ surface are the in-plane oxygen, rather than the top terminal oxygen.

3.4 Comparisons between $WO_3(001)$ surface and the $(WO_3)_n$ clusters

It is well accepted that the structural and electronic properties of metallic clusters less than 50–60 atoms are distinct from their bulk [41]. In contrast to the traditional opinion for the metal system, the transition metal oxide possesses its bulk-like characteristic even in a small cluster [16]. In this section, by comparing the results of stoichiometric $(WO_3)_n$ clusters ($n = 1$–6) with those of the $WO_3(001)$ surface, we want to determine the critical cluster size at which geometric and electronic properties converge to the $WO_3(001)$ surface.

The configurations and electronic structures of some small tungsten oxide clusters have been investigated extensively using photoelectron spectroscopy experiments combined with DFT calculations based on the hybrid B3LYP method with an atomic orbital basis set [14, 16, 42–45]. In this work, the structures of ground state $(WO_3)_n$ clusters with $n = 1$–6 (placed in a $20 \times 20 \times 20$ Å cubic box), which the initial configurations are derived from the results of Li et al. [14], are reexamined at the PW91 level with a plane-wave basis set. As the size of cluster increases, the symmetries of $(WO_3)_n$ clusters are C_{3v}, D_{2h}, D_{3h}, D_{4h}, D_{5h}, and O_h, respectively. The results of geometrical optimization of $(WO_3)_n$ clusters are displayed in Fig. 5, and the data obtained by the hybrid B3LYP method are also given for comparison. It is clear that the configurations predicted by the two approaches are very similar, and the differences among the W–O bond lengths and O–W–O bond angles are smaller than 0.01 Å and 2°, respectively. Except for the smallest WO_3 molecule, there are two kinds of oxygen atoms in $(WO_3)_n$ clusters, one is the terminal oxygen (O_t), and the other is the bridging oxygen (O_b) atoms. Examining the lengths of different W–O bonds, it is obvious that the O_t and O_b atoms in $(WO_3)_n$ cluster are corresponding to the O_{top} and O_{plane} atoms in the $WO_3(001)$ surface, respectively. Some typical structural parameters of clusters are summarized in Table 4. We can see that for the $(WO_3)_n$ clusters with $n = 3$–6, the W–W distance, the lengths of W–O_t and W–O_b bonds are close to the values of $(\sqrt{2} \times \sqrt{2})R45°$ $WO_3(001)$ surface. Therefore, the $(WO_3)_3$ cluster (namely W_3O_9) can be viewed as the smallest cluster bearing surface-like feature from the structural aspect [16].

But if we further consider the electronic structure, what is the critical size for the tungsten oxide clusters bearing a general resemblance to the surface? The atomic DOSs of different $(WO_3)_n$ clusters are shown in Fig. 6, and in here,

we take care the DOSs of two kinds of oxygen atoms in the clusters. For those clusters with $n = 1$–5, the main composition of the "valence band maximum" (namely the highest occupied molecular orbital) is derived from the terminal oxygen atom (O_t), while the contributions of the bridging oxygen atom (O_b) are small. However, it is interesting that in the W_6O_{18} cluster, the $2p$ states of O_b atom become the dominant component of the "valence band maximum", which is analogous to the $WO_3(001)$ surface. The above obvious change of the electronic structure of $(WO_3)_n$ cluster can be attributed to the variation of the relative "compositions" of two kinds of oxygen atoms in the cluster. We note that the cluster presents a planar structure when $n \leq 5$, but the configuration turns to be three-dimensional when $n \geq 6$ (see Fig. 5). Accompany with the structural variation, the ratio between the numbers of O_t and O_b atom in the cluster is also changed. By counting the numbers of O_t and O_b atoms, the O_t/O_b ratio of each system is obtained, and the corresponding values are listed in Table 4. The value of O_t/O_b ratio varies from 2:1 in those clusters (except WO_3) with planar structure to 1:2 in three-dimensional W_6O_{18} cluster. In other words, the clusters with $n \leq 5$ are bridging oxygen-deficient, while W_6O_{18} is the beginning cluster that is bridging oxygen-enriched. Actually, for the $WO_3(001)$ surface, the composition of the top layer is also bridging oxygen-enriched (Fig. 1), and if the half of the top oxygen atoms are not removed, the corresponding O_t/O_b (namely O_{top}/O_{plane}) ratio is exactly 1:2. Because the higher relative proportion of bridging O atom results in the increasing in the repulsive interaction among O_b atoms, the bridging oxygen rather than the terminal one tends to have important contributions to the "valence band maximum" in the systems. Hence, our results demonstrate that the W_6O_{18} is the smallest cluster that possesses both structural and electronic features of the $WO_3(001)$ surface, as well as the relative compositions of two kinds of oxygen atoms.

### 3.5 Adsorptions of BH_3 molecule on $WO_3(001)$ surface and W_6O_{18} cluster

Traditionally, the properties of metal oxides can be described in terms of Lewis acidity and basicity, and the basicities of oxygen atoms with different chemical environments can be investigated using appropriate acidic molecule. In this work, we select BH_3 [46] as a probe molecule to determine the activity of different oxygen atoms in the tungsten trioxide.

The γ-monoclinic $WO_3(001)$ surface with the removing of half of the top oxygen atoms is investigated, and three possible adsorption sites are considered, including the site above the top oxygen atom (O_{top}), the site above the in-plane oxygen atom (O_{plane}), and the site on top of a

Fig. 5 Optimized structures of $(WO_3)_n$ ($n = 1$–6) clusters. The bond lengths are in angstroms and bond angles in degrees. The results obtained by the B3LYP method with an atomic orbital basis set [14] are also listed in *parentheses* for comparisons


(a) WO₃ (C₃ᵥ)

(b) W₂O₆ (D₂ₕ)

(c) W₃O₉ (D₃ₕ)

(d) W₄O₁₂ (D₄ₕ)

(e) W₅O₁₅ (D₅ₕ)

(f) W₆O₁₈ (Oₕ)
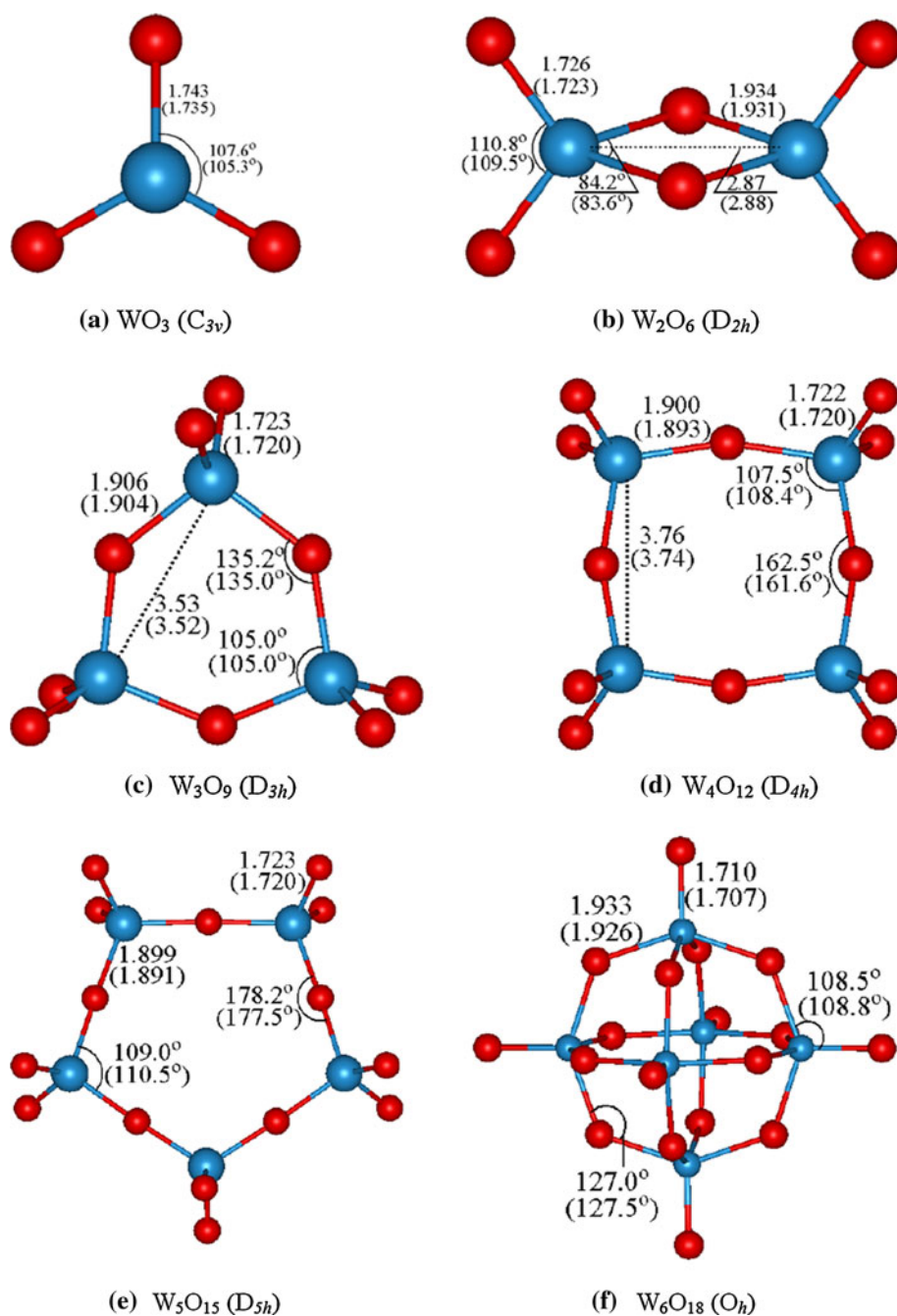
Table 4 Structural parameters of $(WO_3)_n$ ($n = 1$–6) clusters compared with those values of the optimized cubic ($\sqrt{2} \times \sqrt{2})R45°$ and γ-monoclinic WO₃(001) surfaces

Systems	W–W distance (Å)	W–O$_t$ bond length (Å)	W–O$_b$ bond length (Å)	O$_t$/O$_b$ ratio
WO₃	–	1.743	–	3:0
(WO₃)₂	2.87	1.726	1.934	2:1
(WO₃)₃	3.53	1.723	1.906	2:1
(WO₃)₄	3.76	1.722	1.900	2:1
(WO₃)₅	3.79	1.723	1.899	2:1
(WO₃)₆	3.46	1.710	1.933	1:2
Cubic ($\sqrt{2} \times \sqrt{2})R45°$	3.88	1.710	1.982	1:4 (1:2)[a]
γ-Monoclinic	3.87	1.711	1.933	1:4 (1:2)[a]

[a] It is corresponding to the value if the half of the top oxygen atoms are not removed

Fig. 6 Atomic DOSs of $(WO_3)_n$ ($n = 1$–6) clusters. The *vertical dashed line* indicates the position of the highest occupied molecular orbital (*HOMO*), and the inset is the distributions of charge density associated with HOMO
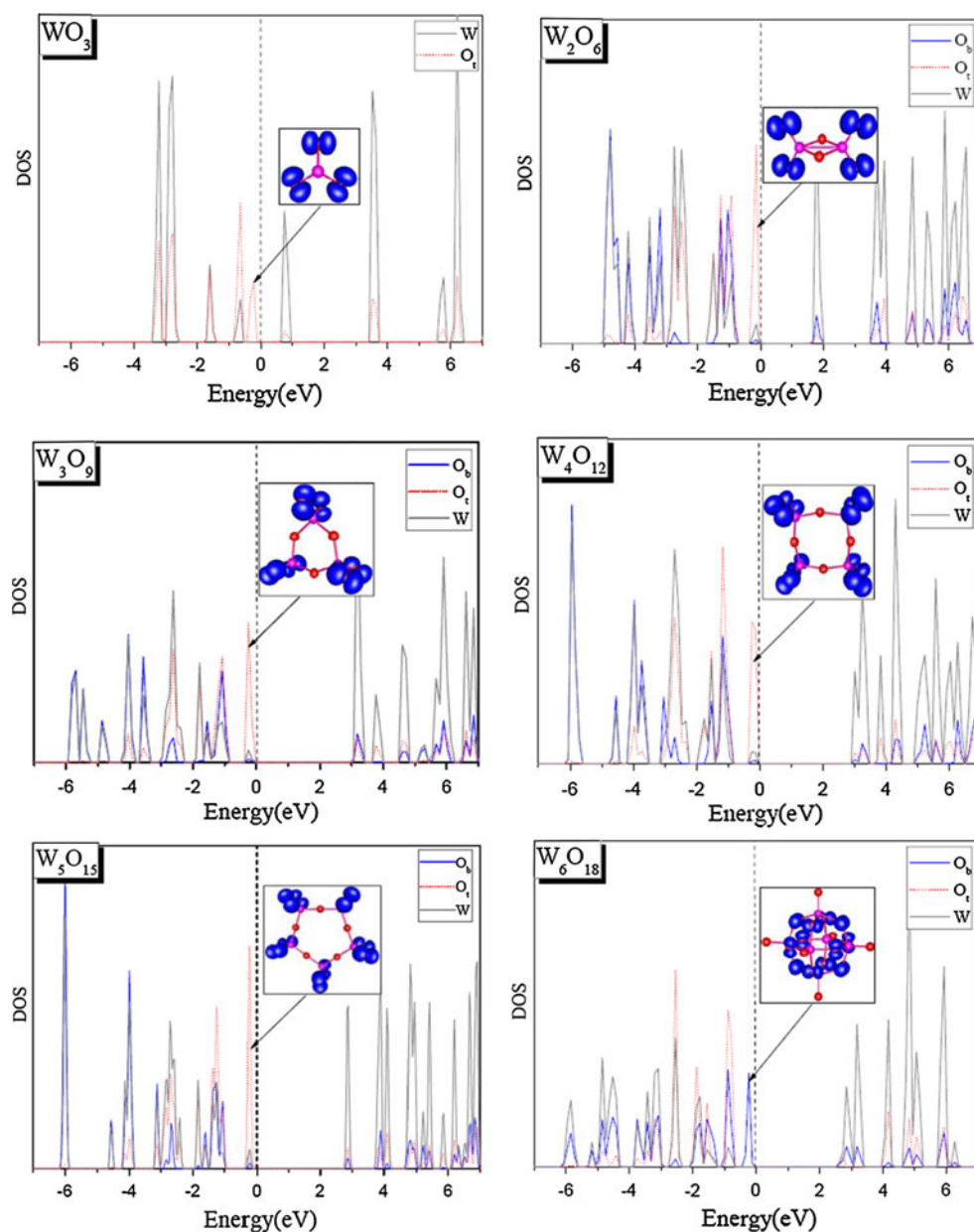
fivefold coordinated tungsten atom (W_{5f}). However, the adsorption on the W_{5f} site does not lead to a stable structure, and geometrical optimization produces only a physisorbed configuration. The final structures for the adsorptions of BH_3 on the O_{top} and O_{plane} sites are displayed in Fig. 7, and the lengths of the corresponding adsorption bonds, B–O_{top} and B–O_{plane}, are 1.479 and 1.556 Å, respectively. Although the B–O bond for site O_{plane} is about 0.08 Å longer than that for site O_{top}, the site O_{plane} is found to be more energetically favorable by 0.28 eV. Therefore, BH_3 molecule preferentially adsorbs on the O_{plane} site of $WO_3(001)$ surface, consisting with the aforementioned result that the in-plane oxygen appears more Lewis basicity than the top terminal oxygen.

How about the adsorption of BH_3 on a W_6O_{18} cluster that has similar electronic structure like $WO_3(001)$ surface? Here, as displayed in Fig. 7c, d, there are two possible adsorption sites, the terminal oxygen and the bridge oxygen. Similar to the $WO_3(001)$ surface, the BH_3 molecule also can be attached to the bridge oxygen atom, and the predicted length of B–O bond (1.526 Å) is close to the value of $WO_3(001)$ surface. In addition, our results indicate that the configuration of the adsorption on the bridge oxygen is about 0.11 eV more stable than the case of adsorption on the terminal oxygen, which is in accord with the result of $WO_3(001)$ surface. Therefore, it can be expected that the bridge oxygen exhibits more activity for electrophilic reagents than the terminal oxygen in the larger

Fig. 7 Optimized configurations for the adsorption of BH$_3$ molecule on the γ-monoclinic WO$_3$(001) surface and W$_6$O$_{18}$ cluster, including the sites **a** above the top oxygen atom and **b** above the in-plane oxygen atom for WO$_3$(001) surface, and **c** on the terminal oxygen atom and **d** on the bridging oxygen atom for W$_6$O$_{18}$ cluster. The bond lengths are in angstroms and bond angles in degrees. In **a** and **b**, only the outmost two layers of surface are shown. The W, O, B, and H atoms are denoted by *blue, red, pink,* and *white balls,* respectively
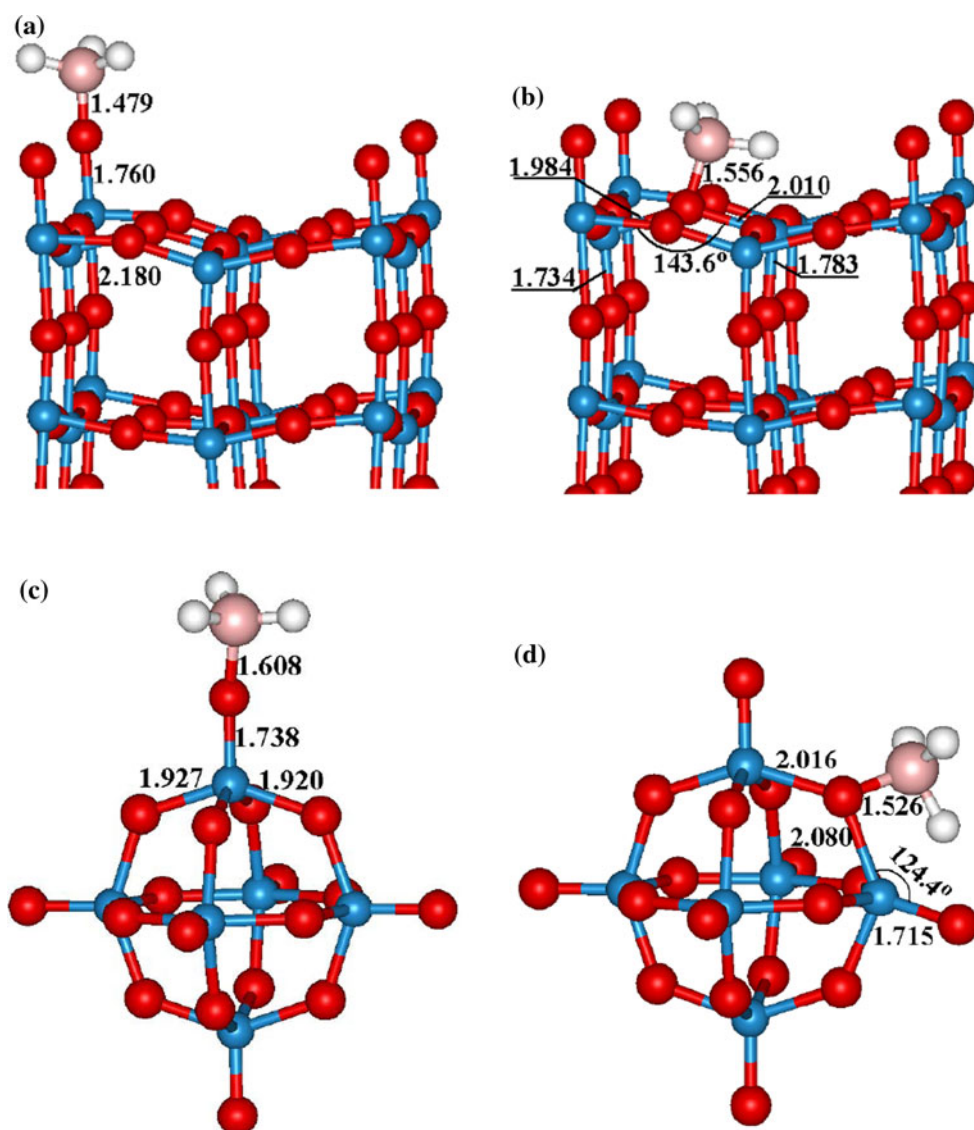
(WO$_3$)$_n$ clusters ($n \geq 6$). Actually, the early experiments have demonstrated that in the tungsten heteropoly acids (W$_{12}$PO$_{40}$$^{3-}$) with the Keggin structure, the preferred alkylation sites are the bridging oxygen rather than the terminal oxygen atoms [47].

4 Conclusions

In this work, the geometries and electronic structures of WO$_3$(001) surface and a series of stoichiometric (WO$_3$)$_n$ clusters have been systematically investigated by first-principles DFT calculations. Six possible reconstructured models of WO$_3$(001) surface with cubic phase are explored, and our results indicate that the ($\sqrt{2} \times \sqrt{2}$)$R45°$ WO$_3$(001) surface is most stable. The surface relaxation of WO$_3$(001) is obvious, and the largest displacement is observed for the W$_{6f}$ atom, which gives rise

to significant changes of the electronic structure of WO$_3$(001) surface. Due to the formation of double bond between W$_{6f}$ and O$_{top}$ atoms, the 2p states of O$_{top}$ tend to keep away from the Fermi level with respect to the unrelaxed surface. Consequently, the top of valence band is dominated by the 2p states of O$_{plane}$ atom, and the in-plane oxygen becomes the preferred site for the nucleophilic reaction occurred on the surface. Although the ideal cubic phase is focused in the present work, this conclusion is also appropriate for the WO$_3$(001) surface with γ-monoclinic phase.

For the (WO$_3$)$_n$ clusters, concerning the bond lengths of two kinds of W–O bonds and the W–W distance, the clusters with $n \geq 3$ possess the geometrical features of WO$_3$(001) surface, so from the structural point of view the W$_3$O$_9$ cluster can be used as the smallest molecular prototype of the WO$_3$ surface. However, in terms of the electronic structure, for those (WO$_3$)$_n$ clusters with planar

framework ($n \leq 5$), including the W_3O_9 species, the highest occupied molecular orbital is mainly composed of the $2p$ orbitals of the terminal oxygen, distinctly differing from the result of $WO_3(001)$ surface. On the other hand, the thing changes for the W_6O_{18} cluster with three-dimensional configuration; now, the bridging oxygen has the dominant contribution for the highest occupied molecular orbital, which is similar to the $WO_3(001)$ surface. By analyzing the compositions of two kinds of oxygen, it is interesting that both W_6O_{18} cluster and $WO_3(001)$ surface are bridging oxygen-enriched, and the similarity in the composition of oxygen atom may be the reason why two systems show analogy in the electronic structures. Therefore, our results imply that when we use a cluster to simulate the surface of metal oxide, the composition of different kinds of oxygen atom must be considered besides the geometrical resemblance. In addition, using BH_3 as a probe molecule, W_6O_{18} and $WO_3(001)$ surfaces bear resemblances to the chemical adsorption of BH_3.

Therefore, according to the results of three aspects: geometry, electronic structure, and the relative composition of different kinds of oxygen, we can conclude that, like a well-known case used a hydrogen ring to represent an infinite hydrogen chain, the W_6O_{18} cluster with a spherical buckyball structure can be considered as a model system to understand the complex processes happened on the $WO_3(001)$ surface.

References

1. Zheng H, Qu JZ, Strano MS, Kaner RB, Mitchell A, Kalantar-zadeh K (2011) Adv Funct Mater 21:2175–2196
2. Corà F, Patel A, Harrison NM, Dovesi R, Catlow CRA (1996) J Am Chem Soc 118:12174–12182
3. Ramana CV, Utsunomiya S, Ewing RC, Julien CM, Becker U (2006) J Phys Chem B 110:10430–10435
4. Radecka M, Sobas P, Wierzbicka M, Rekas M (2005) Phys B 364:85–92
5. Walkingshaw AD, Spaldin NA, Artacho E (2004) Phys Rev B 70:165110-1–165110-7
6. Huda MN, Yan YF, Moon CY, Wei SH, Al-Jassim MN (2008) Phys Rev B 77:195102-1–195102-13
7. Gillet M, Mašek K, Gillet E (2004) Surf Sci 383:566–568
8. Dohnálek Z, Kim J, Bondarchuk O, White JM, Kay BD (2006) J Phys Chem B 110:6229–6235
9. Lebarbier V, Clet G, Houalla M (2006) J Phys Chem B 110:22608–22617
10. Zhu J, Jin H, Chen WJ, Li Y, Zhang YF, Ning LX, Huang X, Ding KN, Chen WK (2009) J Phys Chem C 113:17509–17517
11. Onfroy T, Clet G, Houalla M (2005) J Phys Chem B 109:14588–14594
12. Jena P, Castleman AW Jr (2006) Proc Natl Acad Sci 103:10560–10569
13. Johnson GE, Tyo EC, Castleman AW Jr (2008) Proc Natl Acad Sci 105:18108–18113
14. Li S, David AD (2006) J Phys Chem A 110:6231–6244
15. Huang X, Zhai HJ, Li J, Wang LS (2006) J Phys Chem A 110:85–92
16. Sun Q, Rao BK, Jena P, Stolcic D, Kim YD, Gantefor G, Castleman AW Jr (2004) J Chem Phys 121:9417–9422
17. Tanner RE, Meethunkij P, Altman EI (2000) J Phys Chem B 104:12315–12323
18. Bullett DW (1983) J Phys C Solid State Phys 16:2197–2207
19. Dixon RA, Egdell RG (2000) Surf Sci 452:207–219
20. Tanner RE, Altman EI (2001) J Vac Sci Technol A 19:1502–1509
21. Jones FH, Rawlings K, Foord JS, Egdell RG, Pethica HB, Wanklyn BMR, Parker SC, Oliver PM (1996) Surf Sci 359:107–121
22. Vogt T, Woodward PM, Hunter BA (1999) J Solid State Chem 144:209–215
23. Yakovkin IN, Gutowski M (2007) Surf Sci 601:1481–1488
24. Wang FW, Valentin CD, Pacchioni G (2011) J Phys Chem C 115:8345
25. Dixon RA, Williams JJ, Morris D, Rebane J, Jones FH, Egdell RG, Downes SW (1998) Surf Sci 399:199–211
26. Jones FH, Dixon RA, Brown A (1996) Surf Sci 369:343–350
27. Tasker PW (1979) J Phys C Solid State Phys 12:4977–4984
28. Li M, Posadas A, Ahn CH, Altman EI (2005) Surf Sci 579:175–187
29. Oliver PM, Parker SC, Egdell RG, Jones FH (1996) J Chem Soc Faraday Trans 92:2049–2056
30. Watson GW, Kelsey ET, de-Leeuw NH, Duncan JH, Parker SC (1996) J Chem Soc Faraday Trans 92:433–438
31. Liang S, Mei D, Gutowski M (2011) Catal Today 165:41–48
32. Valdés Á, Kroes G-J (2009) J Chem Phys 130:114701-1–114701-9
33. Kresse G, Furthmüller J (1996) Phys Rev B 54:11169–11186
34. Kresse G, Furthmüller J (1996) Comput Mater Sci 6:15–50
35. Perdew JP, Chevary JA, Vosko SH, Jackson KA, Pederson MR, Singh DJ, Fiolhais C (1992) Phys Rev B 46:6671–6687
36. Monkhorst HJ, Pack JD (1976) Phys Rev B 13:5188–5192
37. Gillet M, Aguir K, Lemire C, Gillet E, Schierbaum K (2004) Thin Solid Films 467:239–246
38. Salje E (1977) Acta Crystallogr B 33:574–577
39. We also have investigated the band structure of the ideal WO3(001) surface by using Becke's three-parameter hybrid functional (B3LYP) combined with atomic orbital basis sets, and a very similar band structure (not shown) is obtained except a relatively large value of the band gap (about 0.87 eV)
40. Bringans RD, Höchst H, Shanks HR (1981) Phys Rev B 24:3481–3489
41. Taylor KJ, Pettiette CL, Cheshnovsky O, Smalley RE (1992) J Chem Phys 96:3319–3329
42. Huang X, Zhai HJ, Waters T, Li J, Wang LS (2006) Angew Chem Int Ed 45:657–660
43. Zhai HJ, Huang X, Cui LF, Li X, Li J, Wang LS (2005) J Phys Chem A 109:6019–6030
44. Zhai HJ, Kiran B, Cui LF, Li X, Dixon DA, Wang LS (2004) J Am Chem Soc 126:16134–16141
45. Rothgeb DW, Hossain E, Kuo AT, Troyer JL, Jarrold CC (2009) J Chem Phys 131:044310–044322
46. Konecny R, Doren DJ (1997) J Phys Chem B 101:10983–10985
47. Knoth WH, Harlow RL (1981) J Am Chem Soc 103:4265–4266